

Charged Higgs bosons in single top production at the LHC

Renato Guedes

Centro de Física Teórica e Computacional, Faculdade de Ciências, Universidade de Lisboa, Av. Prof. Gama Pinto 2, 1649-003 Lisboa, Portugal.

Email: renato@cii.fc.ul.pt

Stefano Moretti

School of Physics and Astronomy, University of Southampton, Highfield, Southampton SO17 1BJ, UK.

Email: stefano@phys.soton.ac.uk

Rui Santos

Instituto Superior de Engenharia de Lisboa, Rua Conselheiro Emídio Navarro 1, 1959-007 Lisboa, Portugal &

Centro de Física Teórica e Computacional, Faculdade de Ciências, Universidade de Lisboa, Av. Prof. Gama Pinto 2, 1649-003 Lisboa, Portugal.

Email: rsantos@cii.fc.ul.pt

ABSTRACT: We show that a light charged Higgs boson signal via $\tau^\pm\nu$ decay can be established at the Large Hadron Collider (LHC) also in the case of single top production. This process complements searches for the same signal in the case of charged Higgs bosons emerging from $t\bar{t}$ production. The models accessible include the Minimal Supersymmetric Standard Model (MSSM) as well a variety of 2-Higgs Doublet Models (2HDMs). High energies and luminosities are however required, thereby restricting interest on this mode to the case of the LHC running at 14 TeV with design configuration.

KEYWORDS: Charged Higgs bosons, LHC, single top.

Contents

1. Introduction	1
2. H^\pm Signal and SM backgrounds	3
3. Selection	5
4. Results and discussion	12
5. Summary, conclusions and outlook	16
A. Cut flow for a 120 GeV charged Higgs boson	17

1. Introduction

The Large Hadron Collider (LHC) is presently operating at a Centre-of-Mass (CM) energy of 8 TeV, following the highly successful stage at 7 TeV, where about 5 fb^{-1} of luminosity were collected. The expectation at present for the current run is a 15 fb^{-1} data sample. In a few years from now, the LHC will be operating at design energy and luminosity, i.e., at 14 TeV and with the prospect of gathering of the order of 300 fb^{-1} or so of data. The highest priority of the CERN machine is to finally confirm, or indeed disprove, the current paradigm for Electro-Weak Symmetry Breaking (EWSB), whereby a Higgs mechanism is postulated to give mass to force and matter states by spontaneously breaking the underlying $SU(2)_L \otimes U(1)_Y$ gauge symmetry (involving isospin L and hypercharge Y) while instead preserving $SU(3)_C$ (where C is colour). While it was first embedded within the Standard Model (SM), wherein the Higgs mechanism is implemented in its minimal form, i.e., through a single Higgs doublet complex field (from which then one scalar Higgs field finally emerges after EWSB), it is now clear that Beyond the SM (BSM) physics is required, given overwhelming experimental evidence that cannot be explained within the SM alone (like neutrino masses, Dark Matter (DM), the matter-antimatter asymmetry, etc.). Conversely, recent LHC evidence of possible neutral Higgs signals at a mass of 124–126 GeV [1, 2], compatible with the SM hypothesis, with a slight excess in the $h \rightarrow \gamma\gamma$ channel, calls for not dismissing the Higgs mechanism as the means for achieving EWSB. So that one may well argue that exploring the possibility of

BSM physics, still reliant on the Higgs hypothesis for EWSB yet with the latter realised in some non-minimal version, has become the main focus at present of the phenomenological activities concerned with LHC data.

One of the most striking evidences of BSM physics employing a non-minimal Higgs mechanism as the source of EWSB would be the appearance of a (singly) charged Higgs boson, H^\pm . The latter is predominantly (but not only) produced in top-(anti)quark decays, so long that it is light, i.e., $m_{H^\pm} < m_t$ (the top mass). Presently, the LEP experiments have set a lower limit on the mass of a charged Higgs boson, of 79.3 GeV at 95% Confidence Level (CL), assuming that $\text{BR}(H^+ \rightarrow \tau^+\nu) + \text{BR}(H^+ \rightarrow c\bar{s}) = 1$ holds for the possible charged Higgs boson Branching Ratios (BRs) [3]. This limit becomes stronger if $\text{BR}(H^+ \rightarrow \tau^+\nu) \approx 1$ (see [4] for a discussion). Searches at the Tevatron [5] based on $t\bar{t}$ production with one of the tops decaying via $t \rightarrow bH^+$ and assuming $\text{BR}(H^+ \rightarrow \tau^+\nu) \approx 1$ have yielded a limit of $\text{BR}(t \rightarrow bH^+) < 0.2$ for a charged Higgs mass of 100 GeV. The LHC is currently providing limits similar to those obtained at the Fermilab machine [6].

The simplest extensions of the SM that give rise to charged Higgs bosons amount to the addition of an extra Higgs doublet to the SM field content. The most common CP-conserving 2HDM has a softly broken Z_2 symmetry. When this symmetry is extended to the fermions to avoid Flavour Changing Neutral Currents (FCNCs) we end up with four [7] different models, which we will call Type I, Type II, Type Y and Type X [8] (named I, II, III and IV in [7], respectively). Constraints from B -physics, and particularly those coming from $b \rightarrow s\gamma$ [9], have excluded a charged Higgs boson with a mass below approximately 300 GeV almost independently of $\tan\beta = v_2/v_1$ – the ratio of the Vacuum Expectation Values (VEVs) of the two doublets – in models Type II and Type Y¹. Charged Higgs bosons with masses as low as 100 GeV are instead still allowed in models Type I and Type X [4, 8, 10].

These scenarios as well as their experimental and theoretical constraints have been discussed in detail in [11], to which we refer the reader also for conventions and notation. In that paper, which reviewed the LHC scope in probing 2HDMs through the detection of a light H^\pm state in all possible production modes, predominantly decaying via $H^\pm \rightarrow \tau^\pm\nu$, one channel was singled out as offering clear prospects of detection, i.e., H^\pm production from top-(anti)quark decays where the latter is produced in single mode, as opposed to the case wherein the top-(anti)quark is produced in pairs, as it was customary to exploit (in fact, successfully) in previous literature. This conclusion was strongly supported in that paper by a detailed parton level analysis, however, the authors of [11] also cautioned that this result should have eventually been put on firmer ground through a full Parton Shower (PS), hadronisation and detector study. Only after this, the yield of the ‘single-top’ channel could be

¹However, if a 2HDM Type II is embedded in Supersymmetry, such a realisation of EWSB remains possible, as the additional sparticle states available, e.g., in the MSSM, can cancel out the H^\pm contributions to B -physics observables.

contrasted with the one obtained through the ‘double-top’ mode and the exclusion and discovery reaches of either channel relatively assessed.

It is the aim of this paper to carry out this PS, hadronisation and detector analysis and to attempt comparing the ensuing new results from ‘single-top’ with the time honoured ones established through ‘double-top’ analyses. In this study we will concentrate on the 14 TeV CM energy because, as it will become clear later on, not only the cross section for the single-top mode grows significantly with energy (in view of its dominant t -channel topology) but also a large amount of luminosity is needed to start probing it at statistically profitable levels. The analysis will be carried out in the context of 2HDMs, however, it is important to note that the phenomenology of a light charged Higgs boson as discussed herein is much more general. There is in fact a large number of BSM Higgs scenarios that share a common charged Higgs boson phenomenology for vast regions of their parameter space with those discussed here. All such models have in common the fact they have a specific type of 2HDM as constituent for achieving EWSB. Recently, a number of these scenarios have been discussed in the literature [12], wherein the charged Higgs boson BR into leptons (including τ ’s) is enhanced relative to the SM case (Type X), which provide DM candidates naturally and can finally accommodate neutrino oscillations as well as the strong first order phase transition required for successful baryogenesis while being in agreement with all experimental data.

The plan of the paper is as follows. The next section describes the main production and decay modes of such a light charged Higgs state at the LHC alongside the corresponding backgrounds. The following one documents our selection strategy and presents our main results. Finally, we conclude in Section 4.

2. H^\pm Signal and SM backgrounds

Although the single-top channel is not the main top-(anti)quark production process at the LHC, it is still significant enough to deserve a full investigation regarding its contribution to the production of charged Higgs bosons. We will mainly focus on a light charged Higgs boson produced via t -channel graphs, $pp \rightarrow t j \rightarrow H^+ \bar{b} j$ and $H^+ \rightarrow \tau^+ \nu$, together with $pp \rightarrow \bar{t} j \rightarrow H^- b j$ and $H^- \rightarrow \tau^- \bar{\nu}$, where j represents a light-quark jet. In what follows we are considering proton-proton collisions at a center-of-mass (CM) energy of $\sqrt{s} = 14$ TeV and a top-quark mass $m_t = 173$ GeV. The theoretical normalisations presented in this section for the different single-top production processes are all through Next-to-Next-to-Leading-Order (NNLO) accuracy, albeit limited to the Next-to-Next-to-Leading-Logarithmic (NNLL) component, as described in [13–15]. We have used higher order normalisations in presenting the forthcoming signal results, as described below.

There are three distinct contributions to single top-production at the LHC. We first consider tW associated production which, at lowest order, is the sum of the two

partonic processes $bg \rightarrow tW^-$ and $\bar{b}g \rightarrow \bar{t}W^+$. The cross section for $\sqrt{s} = 14$ TeV at NNLO and for $m_t = 173$ GeV is given by [13]

$$\sigma_{tW^+}^{\text{NNLO}} = 41.8 \pm 1.0^{+1.5}_{-2.4} \text{ pb} \quad (2.1)$$

where the first uncertainty is from the renormalisation/factorisation scale variation between $m_t/2$ and $2m_t$ and the second is from the MSTW2008 NNLO Parton Distribution Functions (PDFs) [16] at 90% CL. The cross section is the same for both top and antitop production and therefore the sum of the two processes yields 83.6 pb. Second, we consider s -channel production via $q\bar{q}' \rightarrow t\bar{b}$ and $\bar{q}q' \rightarrow \bar{t}b$. The cross sections were calculated in [14]:

$$\sigma_{t\bar{b}}^{\text{NNLO}} = 7.93 \pm 0.14^{+0.31}_{-0.28} \text{ pb} \quad (2.2)$$

and

$$\sigma_{\bar{t}b}^{\text{NNLO}} = 3.99 \pm 0.05^{+0.14}_{-0.21} \text{ pb} \quad (2.3)$$

where uncertainties are as described for eq. (2.1). The total cross section for top plus antitop production via s -channel is then 11.9 pb. However, the most important contribution for single-top at the LHC comes from the aforementioned t -channel process. The total cross section for t -channel top production is in fact [15]

$$\sigma_{tj}^{\text{NNLO}} = 151^{+4}_{-1} \pm 4 \text{ pb} \quad (2.4)$$

while for antitop we have

$$\sigma_{\bar{t}j}^{\text{NNLO}} = 92^{+2+2}_{-1-3} \text{ pb} \quad (2.5)$$

where again the first uncertainty is from scale variation and the second is from the PDFs. The total cross section in t -channel is therefore 243 pb².

The signal consists of the sum of all possible single-top production processes with the subsequent decays $t \rightarrow H^+ b \rightarrow \tau^+ \nu b$ plus all the antitop counterparts with decays $\bar{t} \rightarrow H^- \bar{b} \rightarrow \tau^- \bar{\nu} \bar{b}$. Taking into account the LEP bounds on the mass of a charged Higgs boson, we consider a mass ranging from 90 to 160 GeV and the analysis is performed in 10 GeV mass steps. In order to maximise the signal-to-background significance (S/\sqrt{B}), it turns out that both the s -channel and the tW single-top production modes become negligible. Therefore, when discussing the signal, it is in fact to the t -channel process that we will be referring to, as it is the only one that survives the set of cuts imposed. The signal (single-top) events were generated with POWHEG [17] at NLO with the CTEQ6.6M [18] PDFs. The top was then decayed in PYTHIA [19]. We have considered only the leptonic decays of the tau-leptons, that is, the signal final state is $pp \rightarrow lbj\cancel{E}$, where $l = e, \mu$ (electrons and muons) while \cancel{E} means missing (transverse) energy.

²By comparison, note that the NLO cross section for $t\bar{t}$ production at the LHC is about 800 pb.

The irreducible background to this process is obviously single-top production with the subsequent decay $t \rightarrow bW^+$. Again, all single-top production processes, also generated with POWHEG, were included. We have taken into account the most relevant contributions to the reducible background too: i.e., $t\bar{t}$ production, $W^\pm + \text{jets}$ (including not only light quarks and gluons, but also c - and b -quarks) and the pure QCD background ($j\bar{j}$, where j is any jet), which we will now discuss in turn. The $t\bar{t}$ background was generated with POWHEG including the top and W^\pm boson decays to all possible final states. The $W^\pm + \text{jets}$ (1, 2 and 3 jets) noise was generated with AlpGen [20] with CTEQ6ll PDFs. Finally, the QCD background was generated with CalcHEP [21] and, as before, the CTEQ6ll PDFs were used.

The hadronisation was performed with PYTHIA 6. The Perugia tune [22] was used to handle the underlying events in POWHEG while the ATLAS MC09 tune [23] was used for events generated with AlpGen and CalcHEP. We also have cross-checked the single-top event generation with AcerMC [24] and the $W^\pm + \text{jets}$ events were also generated with MCFM [25, 26] (whose normalisation we have used). To avoid double counting in the $W^\pm + \text{jets}$ background, we have used the MLM matching scheme [27]. Following [27], we have used the following cuts in generation: all jets have transverse momentum above 20 GeV, $|\eta_j| < 2.5$ and $\Delta R_{jj} > 0.7$ while the missing (transverse) energy has to be larger than 20 GeV³.

After hadronisation, DELPHES [28], which is a framework for the fast simulation of a generic collider experiment, was used to simulate the detector effects. For the detector and trigger configurations, we resorted to the ATLAS default definitions.

3. Selection

In this section we describe the analysis and the selection cuts in detail. First we have used the trigger card in ATLAS which for our purposes means that we have asked for an isolated electron with $p_T > 25$ GeV or an isolated muon with $p_T > 20$ GeV. We will now describe the analysis in detail and we start by noting that the pure QCD background is not shown in the plots due to its (initially) overwhelming magnitude. However, we will highlight the selection cuts that have eliminated this background.

1. We demand one electron with transverse momentum larger than 30 GeV or a muon with transverse momentum above 20 GeV. In both cases, the lepton has to be in the central region of the detector, $|\eta| < 2.5$. In the left panel of figure 1 we show the leptonic multiplicity before these cuts.
2. We veto events with two or more leptons with transverse moment above 10 GeV.

In the right panel of figure 1 we show the leptonic multiplicity before such a

³We also have (slightly) changed the cuts at generation level to make sure that no systematic bias was introduced by these, by confirming that only the efficiency of generating the ensuing hadronic final states changed, not their yields.

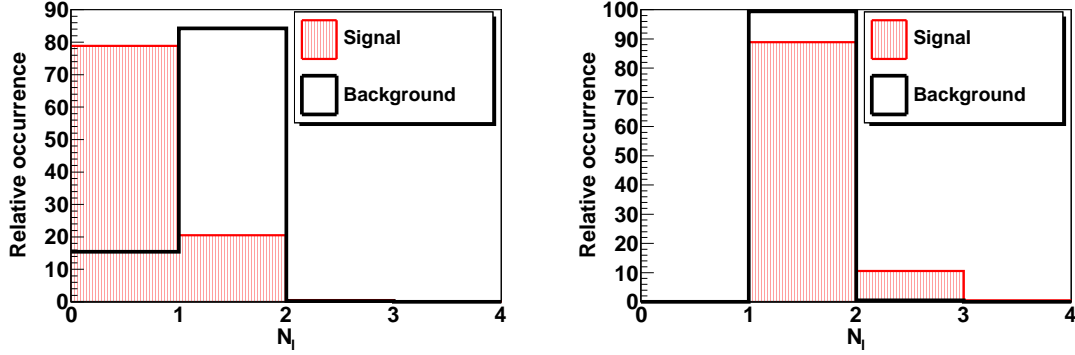


Figure 1: In the left panel we present the number of muons with $p_T > 20$ GeV or the number of electrons with $p_T > 30$ GeV before the first cut. On the right we show the number of leptons with a transverse momentum of at least 10 GeV passing the first cut.

veto. Although the figure seems to indicate that events with two leptons in the final state should be retained, the subsequent cuts show that the background would rise sharply above the signal, should this have been the case. This cut eliminates the leptonic $t\bar{t}$ background almost completely.

3. In figure 2 (left) we show the lepton transverse momentum distribution after imposing the first two cuts. Due to overwhelming W+0 jets background, it is not clear that the best choice to maximise the sensitivity is to exclude events with leptons having p_T above 55 GeV.

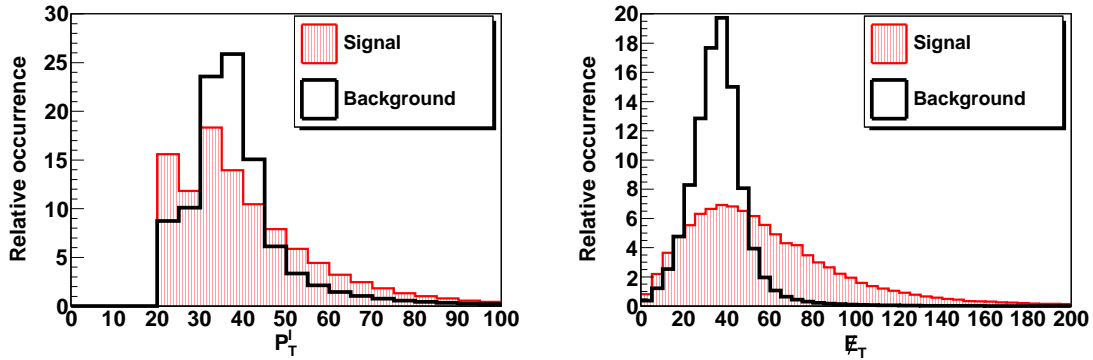


Figure 2: In the left panel the leptons transverse momentum distribution is shown, after imposing both the first and second cut. In the right panel we present the missing transverse energy distribution after the first two cuts.

4. In the right panel of figure 2 we present the missing transverse energy distribution after the first two cuts. We have therefore imposed that events with

missing energy below 50 GeV should be excluded. This is another cut that dramatically reduces the QCD background.

5. In figure 3 (left) we display the number of b -tagged jets after the first four cuts while in the right panel we show the b -tagged jets transverse momentum distribution. We ask for one and only one b -tagged jet with a transverse momentum below 75 GeV. Again, although two b -tagged jets have a higher relative occurrence in signal events, the latter drops significantly once the subsequent cuts are imposed. We assume for each b -tagging efficiency of a b -quark jet the value $R = 0.7$, while for the case of c -quark jets we take 0.1 and for light-quark/gluon jets we adopt 0.01. The background in question is the semi-leptonic $t\bar{t}$ background.

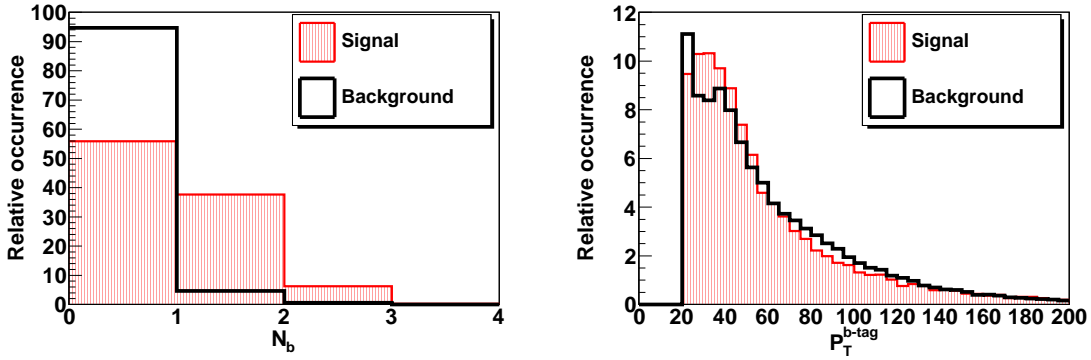


Figure 3: The b -jet selection cuts: number of b -tagged jets with at least 30 GeV (left) and b -tagged jet transverse momentum distribution (right).

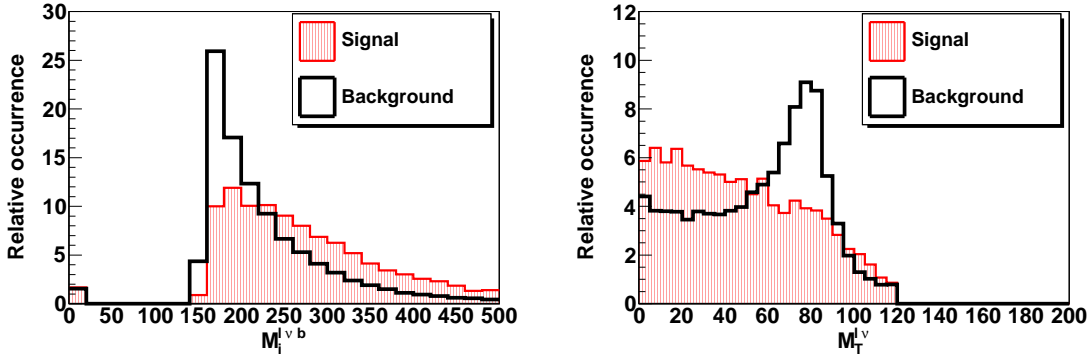


Figure 4: The “top quark invariant mass” distribution (left) and leptonic transverse invariant mass distribution (right).

6. In order to reconstruct the top mass we proceed in the following way. As we do not know the longitudinal component of the missing energy, we look for that

component of the missing energy that together with the lepton momentum reconstructs the charged Higgs mass according to the relation

$$\not{p}_z = \frac{-b \pm \sqrt{b^2 - 4ac}}{2a}, \quad (3.1)$$

where

$$a = \left(\frac{p_{zl}}{p_l} \right)^2 - 1, \quad (3.2)$$

$$b = 2 \left(\frac{p_{xl}\not{p}_x + p_{yl}\not{p}_y}{p_l} + \frac{m_{H^+}^2}{2p_l} \right) \frac{p_{zl}}{p_l}, \quad (3.3)$$

$$c = \left(\frac{p_{xl}\not{p}_x + p_{yl}\not{p}_y}{p_l} + \frac{m_{H^+}^2}{2p_l} \right)^2 - \not{p}_T^2. \quad (3.4)$$

Here, the \not{p}_i 's are the missing energy momentum components, p_{il} are the lepton momentum components, p_l is the (massless) lepton energy and \not{p}_T is the transverse missing energy. With this information we can now reconstruct a “top quark invariant mass”. Of course, because we will reconstruct fake top masses, there is a wide distribution that includes unphysical masses. This distribution is presented in the left panel of figure 4. Whenever we obtained an imaginary value for \not{p}_z , the corresponding events were placed in the 0 – 20 GeV bin. Between the two solutions of eq. (3.1) we have chosen the one that gave a “top quark invariant mass” closest to the top quark mass experimental value. Finally, we demand events to have a “top quark invariant mass” above 280 GeV.

7. Next, we define the leptonic transverse mass [29] as

$$M_T^{l\nu} = \sqrt{2p_{Tl}\not{p}_T - 2(p_{xl}\not{p}_x + p_{yl}\not{p}_y)}, \quad (3.5)$$

where p_{Tl} is the lepton transverse momentum. The leptonic transverse mass distribution is shown in figure 4 (right). To maximise the significance we have accepted events with $30 \text{ GeV} < M_T^{l\nu} < 60 \text{ GeV}$ for charged Higgs masses between 90 and 130 GeV and $30 \text{ GeV} < M_T^{l\nu} < 60 \text{ GeV}$ or $M_T^{l\nu} > 85 \text{ GeV}$ for higher values of the charged Higgs mass. Again, figure 4 (right) would lead us to include values of $M_T^{l\nu}$ below 30 GeV. However, we have excluded events with $M_T^{l\nu} < 30 \text{ GeV}$ to further reduce the pure QCD background.

8. In the left panel of figure 5 we present the jet multiplicity for jets with transverse momentum above 30 GeV and $|\eta| \leq 4.9$. From the figure we would choose events with either one or two jets. However, and again due to the QCD background, we have chosen events with one and one jet only.

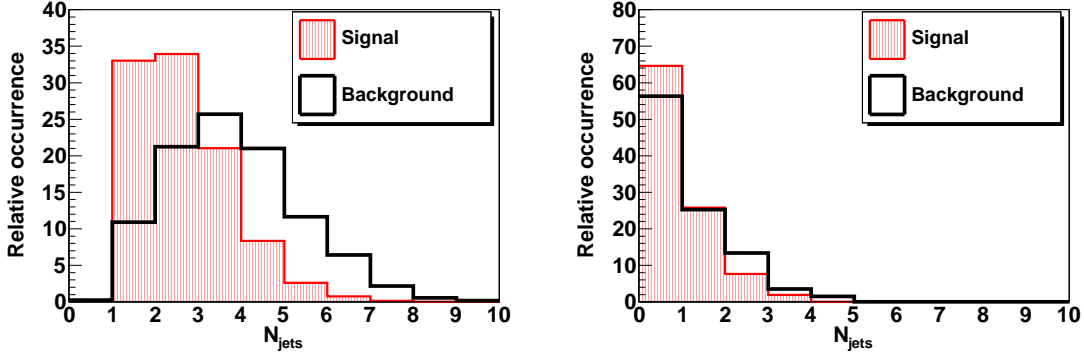


Figure 5: On the left we present the number of jets with transverse momentum above 30 GeV. On the right we show the number of jets that passed the previous cut and have one more jet with a transverse momentum between 15 GeV and 30 GeV. In both cases we require the jet pseudorapidity to be less the 4.9 in absolute value.

9. In figure 5 (right) we present the jet multiplicity after the previous cuts, for jets with $p_T > 15$ GeV and $|\eta| \leq 4.9$. Taking into account the previous cuts, this is the jet multiplicity for jets with transverse momentum between 15 and 30 GeV. We veto all events with a jet multiplicity equal to two or above.

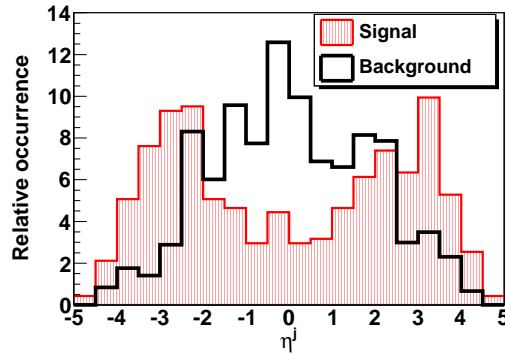


Figure 6: The jet pseudorapidity distribution. (Notice that after the previous cuts there is only one jet with $p_T > 30$ GeV and $|\eta| \leq 4.9$.)

10. Finally, in figure 6 we present the jet pseudorapidity distribution. The last cut is to accept events where jets have a pseudorapidity $|\eta| \geq 2.5$.

We have chosen a charged Higgs mass of 120 GeV to show the result of the analysis after all cuts have been applied (a complete cut flow is presented in Appendix A). In table 1 we list all backgrounds considered in the analysis before and after cuts for a luminosity of 1 fb^{-1} . Clearly, after all cuts have been applied, the main

Process	Events (1 fb ⁻¹)	Events (1 fb ⁻¹)	Efficiency (%)
	before cuts	after cuts	
Single top (<i>t</i> -channel)	246600	18.5	0.0075
Single top (<i>s</i> -channel)	10650	0	0
Single top (<i>tW</i>)	66000	0.7	0.0010
<i>t</i> \bar{t} (semileptonic)	371133	0	0
<i>t</i> \bar{t} (leptonic)	88940	1.8	0.0020
<i>t</i> \bar{t} (hadronic)	387169	0	0
W+0j	4.3×10^7	0	0
W+1j	8.8×10^6	0.6	7.1×10^{-6}
W+2j	2.8×10^6	3.9	0.00014
W+3j	1.2×10^6	0	0
Wc+0j	7.4×10^5	0	0
Wc+1j	3.2×10^5	3.2	0.0010
Wc+2j	2.0×10^5	1.0	0.0011
Wc+3j	8.9×10^4	0	0
Wbb+0j	6638	0	0
Wbb+1j	6582	0.5	0.007
Wbb+2j	3746	0	0
Wbb+3j	2896	0	0

Table 1: Number of background events before and after cuts, alongside the same rates for the signal assuming a charged Higgs mass of 120 GeV.

background is still the single top background while the contributions $W + 2j$ and $W + 1j$ ($j = \text{jet}$) are the most important ones from the reducible background. Given the very low efficiencies, the initial number of events generated for each individual background process was chosen in such a way that the error in the total number of signal events is below 5%. This is done by decreasing the weight of each event until the required precision is attained.

In all backgrounds generated with AlpGen at LO, the renormalisation and factorisation scales were chosen so that total cross section for LO and NLO were similar [30]. After all cuts have been applied we have recalculated the LO and NLO total cross sections and found that the K factors were always of the order 1 or smaller.

In table 2 we show the number of events before and after all cuts as a function of the charged Higgs mass. Recall that signal means all the events produced in $pp \rightarrow tj \rightarrow bH^\pm j$ with $H^\pm \rightarrow \tau\nu \rightarrow l\cancel{E}$, where l is a lepton and \cancel{E} is the transverse missing energy. However, in order, to use these numbers in a variety of models (to be discussed later on) we have taken $\text{BR}(t \rightarrow bH^\pm) = 100\%$ and $\text{BR}(H^\pm \rightarrow \tau^\pm \nu) = 100\%$ and all other BRs have the usual SM values. Also notice that the discontinuity

in the number of events after cuts for a mass of 130 GeV is due to the addition of the selection cut $M_T^{l\nu} > 85$ GeV for charged Higgs masses above 130 GeV.

m_H^\pm (GeV)	Efficiency (%)
90	0.016
100	0.016
110	0.018
120	0.019
130	0.017
140	0.048
150	0.049
160	0.044

Table 2: Signal efficiency considering $\text{BR}(t \rightarrow bH^\pm) = 100\%$ and $\text{BR}(H^- \rightarrow \tau^- \nu) = 100\%$ and all other BRs have the usual SM values.

Putting all the numbers together we can find S/B and S/\sqrt{B} as a function of the charged Higgs mass as presented in table 3.

m_H^\pm (GeV)	Signal (S)	Background (B)	S/B (%)	S/\sqrt{B}
90	38.6	29.5	130.92	7.11
100	40.5	29.5	137.19	7.45
110	45.6	29.8	153.00	8.35
120	47.7	30.1	158.26	8.69
130	42.3	32.68	129.53	7.41
140	117.1	77.9	150.25	13.26
150	120.0	86.6	138.64	12.90
160	109.7	100.8	108.81	10.92

Table 3: Signal-to-Background ratio (S/B) and significance (S/\sqrt{B}) as a function of the charged Higgs mass. The numbers presented for the signal we take $\text{BR}(t \rightarrow bH^\pm) = 100\%$ and $\text{BR}(H^- \rightarrow \tau^- \nu) = 100\%$ and all other BRs have the usual SM values.

Just to give an idea how these numbers are modified for the different models we have chosen two reference points: one for model II, with $\tan \beta = 1$ and one for model type X for $\tan \beta = 3$. In the first case we obtain $S/\sqrt{B} = 1.4$ and $S/B = 25\%$ while in the second the values are $S/\sqrt{B} = 0.3$ and $S/B = 5\%$. How the values of the branching ratios affect the results in the different models will be shown in the exclusion plots presented in the next section.

4. Results and discussion

We start by presenting our results in a model independent manner, where only the τ lepton decays according to the SM branching fractions are considered. Besides, we also consider the top production cross section to be the SM one and because the results are presented for a definite collected luminosity, the exclusion limits are presented for $\text{BR}(t(\bar{t}) \rightarrow H^\pm b) \text{BR}(H^\pm \rightarrow \tau^\pm \nu_\tau)$. To obtain the 95% CL limits we use a code briefly described in [31] which is based on a ROOT library. In the left panel of figure 7 we show the 95% CL limit for $\text{BR}(t(\bar{t}) \rightarrow H^\pm b) \text{BR}(H^\pm \rightarrow \tau^\pm \nu_\tau)$ as a function of the charged Higgs mass with an integrated luminosity of 10 fb^{-1} and for $\sqrt{s} = 14 \text{ TeV}$. In the same figure on the right, we show the results for an integrated luminosity of 30 fb^{-1} instead.

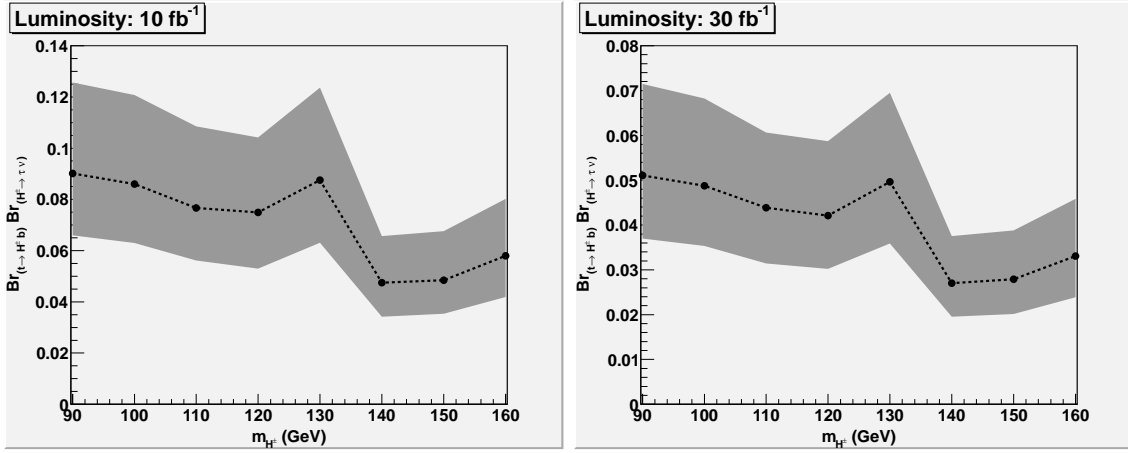


Figure 7: Left: exclusion limits for $\text{BR}(t(\bar{t}) \rightarrow H^\pm b) \text{BR}(H^\pm \rightarrow \tau^\pm \nu_\tau)$ as a function of the charged Higgs mass at 95% CL for 10 fb^{-1} of integrated luminosity. Right: exclusion limits for $\text{BR}(t(\bar{t}) \rightarrow H^\pm b) \text{BR}(H^\pm \rightarrow \tau^\pm \nu_\tau)$ as a function of the charged Higgs mass at 95% CL for 30 fb^{-1} of integrated luminosity.

In figure 8 we present the same limits for an integrated luminosity of 50 fb^{-1} (left) and 100 fb^{-1} (right).

The results presented for $\text{BR}(t(\bar{t}) \rightarrow H^\pm b) \text{BR}(H^\pm \rightarrow \tau^\pm \nu_\tau)$ can be used to constrain any model where the top decays to a charged Higgs boson which subsequently decays to $\tau^\pm \nu_\tau$. The predicted exclusion bounds can be compared to similar plots presented by the ATLAS [32] and CMS [33] collaborations for the 7 TeV run and for the $t\bar{t}$ mode. The ATLAS (CMS) collaboration has an exclusion that ranges from 5 (4) % to a charged Higgs mass of 90 GeV to 1 (2) % for a mass of 160 GeV. We note once more that the search for a charged Higgs in single top production does not and cannot compete with the $t\bar{t}$ search. Its purpose is to be combined with the $t\bar{t}$ results to improve the sensitivity in charged Higgs boson searches.

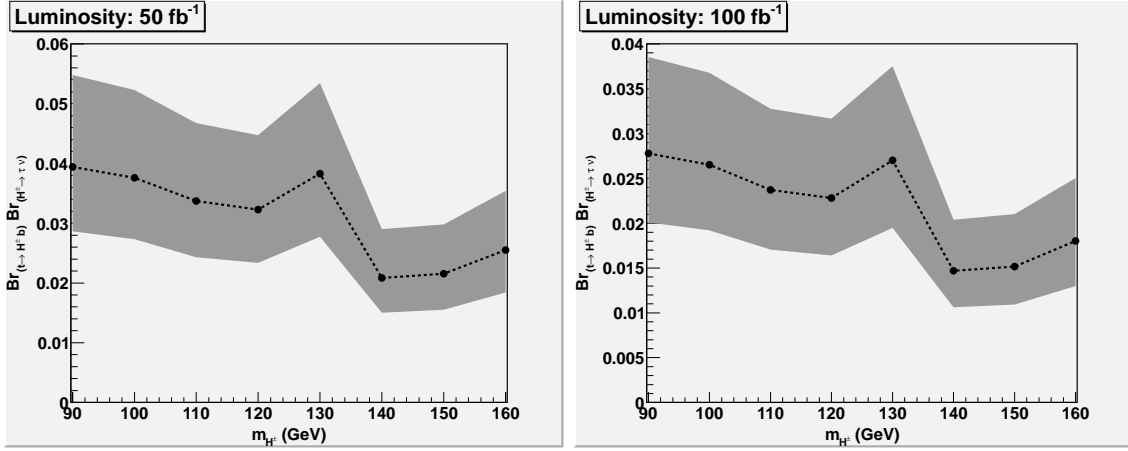


Figure 8: Left: exclusion limits for $\text{BR}(t\bar{t} \rightarrow H^\pm b) \text{BR}(H^\pm \rightarrow \tau^\pm \nu_\tau)$ as a function of the charged Higgs mass at 95% CL and 50 fb^{-1} of integrated luminosity. Right: exclusion limits for $\text{BR}(t\bar{t} \rightarrow H^\pm b) \text{BR}(H^\pm \rightarrow \tau^\pm \nu_\tau)$ as a function of the charged Higgs mass at 95% CL and 100 fb^{-1} of integrated luminosity.

There are several models that we can explore now. Both the MSSM and several versions of 2HDMs have a similar Yukawa Lagrangian in what concerns the charged Higgs boson couplings to fermions. In fact, 2HDM types with a softly broken Z_2 symmetry, $\Phi_1 \rightarrow \Phi_1$, $\Phi_2 \rightarrow -\Phi_2$, either CP-conserving or CP-violating (either explicit or spontaneous) can be written in general terms as

$$V(\Phi_1, \Phi_2) = m_1^2 \Phi_1^\dagger \Phi_1 + m_2^2 \Phi_2^\dagger \Phi_2 + (m_{12}^2 \Phi_1^\dagger \Phi_2 + \text{h.c.}) + \frac{1}{2} \lambda_1 (\Phi_1^\dagger \Phi_1)^2 + \frac{1}{2} \lambda_2 (\Phi_2^\dagger \Phi_2)^2 + \lambda_3 (\Phi_1^\dagger \Phi_1) (\Phi_2^\dagger \Phi_2) + \lambda_4 (\Phi_1^\dagger \Phi_2) (\Phi_2^\dagger \Phi_1) + \frac{1}{2} \lambda_5 [(\Phi_1^\dagger \Phi_2)^2 + \text{h.c.}] , \quad (4.1)$$

where Φ_i , $i = 1, 2$ are complex $SU(2)$ doublets with four degrees of freedom each. The parameters m_{12}^2 , λ_5 and the nature of the VEVs will determine the CP nature of the model (see [34] for a review on the different 2HDMs). Note that hermiticity of the potential forces the remaining parameters to be real. This, in turn, will give rise to different neutral scalar sectors: if CP is conserved we end up with two CP-even Higgs states, usually denoted by h and H , and one CP-odd state, usually denoted by A ; otherwise we will just have three spinless states with undefined CP quantum numbers usually denoted by h_1 , h_2 and h_3 . However, as long as the VEV does not break the electric charge, which was shown to be possible in any 2HDM [35], there are in any case two (identical) charged Higgs boson states, one charged conjugated to the other.

For definiteness, we will concentrate on two specific realisations, one CP-conserving and the other explicitly CP-violating [36–39], and both are free from tree-level FCNCs. In the CP-violating version m_{12}^2 and λ_5 are complex and $\text{Im}(\lambda_5) =$

Model	$g_{\bar{u}dH^+}$	$g_{l\bar{\nu}H^+}$
I	$\frac{ig}{\sqrt{2}M_W}V_{ud}[-m_d/\tan\beta P_R + m_u/\tan\beta P_L]$	$\frac{ig}{\sqrt{2}M_W}[-m_l/\tan\beta P_R]$
II	$\frac{ig}{\sqrt{2}M_W}V_{ud}[m_d\tan\beta P_R + m_u/\tan\beta P_L]$	$\frac{ig}{\sqrt{2}M_W}[m_l\tan\beta P_R]$
Y	$\frac{ig}{\sqrt{2}M_W}V_{ud}[m_d\tan\beta P_R + m_u/\tan\beta P_L]$	$\frac{ig}{\sqrt{2}M_W}[-m_l/\tan\beta P_R]$
X	$\frac{ig}{\sqrt{2}M_W}V_{ud}[-m_d/\tan\beta P_R + m_u/\tan\beta P_L]$	$\frac{ig}{\sqrt{2}M_W}[m_l\tan\beta P_R]$

Table 4: Charged Higgs Yukawa couplings to up-, down-type quarks and leptons.

$2\text{Im}(m_{12}^2)$. In both models the VEVs are real. By defining $\tan\beta = v_2/v_1$, it is then possible to choose the angle β as the rotation angle from the group eigenstates to the mass eigenstates in the charged Higgs sector. By then extending the Z_2 symmetry to the Yukawa sector we end up with four independent 2HDMs, i.e., the aforementioned Type I, Type II, Type Y and Type X, whose H^\pm couplings to fermions are presented in table 4. Herein, P_L and P_R are the left- and right-helicity projection operators, respectively. Further, notice that the vertices $g_{u\bar{d}H^-}$ and $g_{l\bar{\nu}H^-}$ are obtained from the corresponding ones $g_{\bar{u}dH^+}$ and $g_{l\bar{\nu}H^+}$ by interchanging $P_L \leftrightarrow P_R$ and by replacing $V_{ud} \rightarrow V_{ud}^*$.

With this parametrisation the results presented here depend only on $\tan\beta$ and m_{H^\pm} . This is true both for $\text{BR}(t(\bar{t}) \rightarrow H^\pm b)$ and $\text{BR}(H^\pm \rightarrow \tau^\pm \nu_\tau)$. The experimental bounds on the CP-violating model, which for the charged sector are also valid for the CP-conserving one, were recently reviewed in [40]. Taking into account these bounds we have finally looked for the 95% CL exclusion limits in each model.

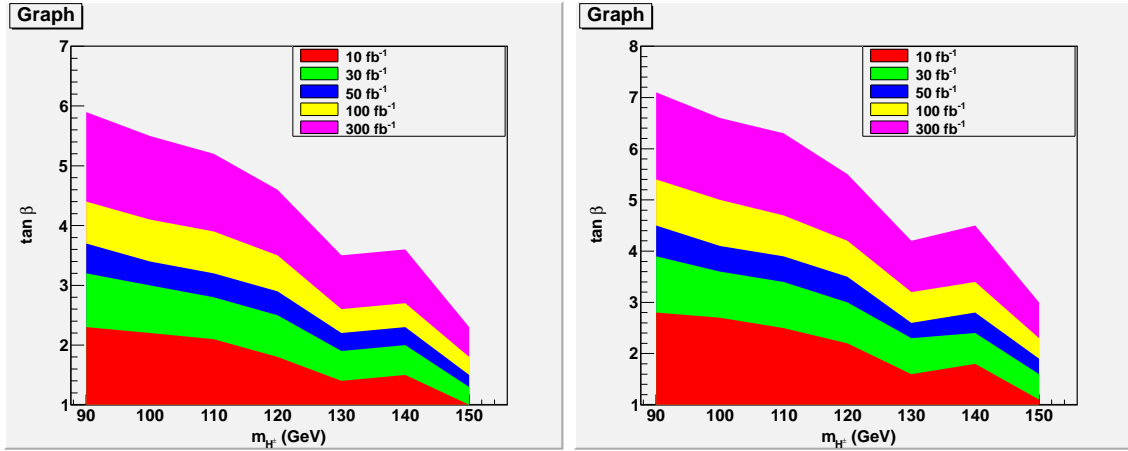


Figure 9: The 2HDM Type I (left) and Type X (right) exclusion limits over the $(\tan\beta, m_{H^\pm})$ plane at the 95% CL assuming the LHC at 14 TeV and for several luminosity sets.

In figure 9 we present the 95% CL exclusion limits for a 2HDM Type I (left) and Type X (right). These results should now be compared with the predictions for $\sqrt{s} = 14$ TeV made by the experimental collaborations at CERN [41, 42]. Using the

ATLAS analysis presented in [41] we can draw exclusion plots for the different models as presented in [11]. Using Type I as an example, ATLAS sets a limit $\tan \beta < 9$ for a collected luminosity of 30 fb^{-1} and for a charged Higgs mass of $m_{H^\pm} = 90 \text{ GeV}$. Figure 9 shows that for the same luminosity we obtain a limit slightly above 3 for $\tan \beta$. For other masses the result is slightly better but the general trend is a factor between 2 and 3 in the ratio of the limits obtained in the two analysis. It should be noted that the ATLAS analysis considers both the leptonic and hadronic decays of the τ leptons reaching, also for that reason, a much higher sensitivity.

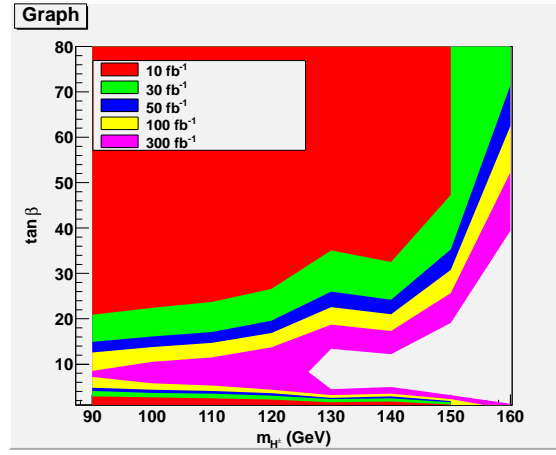


Figure 10: The MSSM exclusion limits over the $(\tan \beta, m_{H^\pm})$ plane at the 95% CL. assuming the LHC at 14 TeV and for several luminosity sets.

In figure 10 we present the 95% CL exclusion limits for a 2HDM Type II, which for phenomenological purposes we may assume it to be the MSSM, so as have the light charged Higgs boson considered here compliant with the $b \rightarrow s\gamma$ constraints. Again these results should be compared with the 14 TeV predictions for the LHC in the $t\bar{t}$ production channel. For comparison purposes, let us consider figure 10 and the exclusion region for 30 fb^{-1} . The allowed region for $m_{H^\pm} = 90 \text{ GeV}$ is for $4.1 < \tan \beta < 14.9$ while our best result is for $m_{H^\pm} = 140 \text{ GeV}$ where the allowed range of $\tan \beta$ at 95% CL is $2.3 < \tan \beta < 24.2$. The ATLAS prediction [41] for the same energy and for the same collected luminosity and considering only the leptonic decays of the τ lepton is $7.1 < \tan \beta < 9.3$ for $m_{H^\pm} = 90 \text{ GeV}$ and is $3.2 < \tan \beta < 21.9$ for $m_{H^\pm} = 130 \text{ GeV}$ at 95% CL. Therefore, it is clear that the results obtained in the single top analysis should be combined with the ones from $t\bar{t}$ production to improve the sensitivity. We note however that this comparison is made with the leptonic mode in the $t\bar{t}$ and when all the τ decay modes are combined the result obviously improves as presented in [41].

Finally, in comparing the results in figures 9 and 10, it should be noticed that there is sensitivity up to $\tan \beta = 70$ in the 2HDM Type II (herein the MSSM)

whereas this is only up to 7 in the case of a 2HDM Type I or Type IV. This is because in the Type I and Type IV case the cross section times BR rates always decrease with an increase of $\tan\beta$, while in Type II the cross section times BR rates decrease with an increase of $\tan\beta$ from 1 to some point, 6 or 7, then they start to increase again.

5. Summary, conclusions and outlook

Now that a neutral Higgs boson signal may be about to be found at the LHC, it becomes of paramount importance to assess the dynamics of the underlying Higgs mechanism of EWSB. In fact, early data (and possibly late ones to appear soon) seem to hint that the excess is above the SM expectations, at least in the (most prominent, for the extracted mass of ≈ 125 GeV) $\gamma\gamma$ decay mode. Therefore, a non-minimal Higgs sector may be required. If the latter involves at least another Higgs doublet, then a (singly) charged Higgs boson is bound to appear in the model spectrum. Of particular phenomenological relevance are 2HDMs, where one and only one complex Higgs doublet is added to the SM one. Herein, there is only one charged Higgs boson state and its mass can be predicted (through unitarity) to be well within the kinematic reach of the LHC. In fact, it is the low mass regime, i.e., $m_{H^\pm} < m_t$, which is the spectacular one, as such a light charged Higgs boson can be generated in top-(anti)quark decays, since the latter are copiously produced at the LHC through efficient QCD interactions.

While past literature exploring the scope of the LHC in the search for light charged Higgs bosons in 2HDMs has concentrated exclusively on the case of H^\pm production from t -(anti)quarks produced in pairs, we have tackled here the case of single-top production, whose cross section is in fact comparable (albeit smaller) to that of double-top production, at all LHC energies. We have found that, when searched for in leptonic decays of primary $\tau\nu$ pairs, the LHC is very sensitive to such a light charged Higgs boson, in the most common (and still viable) realisations of 2HDMs, including the one whose Higgs sector is naturally embedded in Supersymmetry, the so-called MSSM. We have in fact quantified this in terms of exclusion regions, particularly in the MSSM, and proved that single-top production offers an alternative means (albeit of more limited scope) to double-top production to test the existence of otherwise of light H^\pm states. This is most efficiently done at 14 TeV, assuming standard luminosity samples. In this respect, the main highlights are that our results are a factor between 2 and 3 below the ones obtained by ATLAS and CMS for the $t\bar{t}$ production channel. Therefore they can be combined to provide improved exclusion regions for the parameter space of the models. Although not presented by ATLAS and CMS we can state that regarding discovery even for 300 fb^{-1} and for a charged Higgs mass of 100 GeV we can barely reach $\tan\beta = 3$ for Types I and X (and lower limit for Type II) while for higher masses the discovery limit is only possible

for a $\tan\beta \mathcal{O}(1)$. Our conclusions are supported by a thorough phenomenological investigation of signal and both reducible and irreducible backgrounds, in presence of PS, hadronisation and detector effects.

Having proved the accessibility of charged Higgs production in single top mode at the LHC, possible outlooks include now the following.

1. The investigation of the Cabibbo-Kobayashi-Maskawa structure of the $H^\pm tb$ vertex, which in single top mode appears at production level, unlike in the double top channel where such a vertex only enters the top decay, thereby affording more sensitivity to experimental measurements.
2. Because of such a sensitivity at production level to this coupling, one can also attempt extracting the coefficients of the two chiral structures $(1 \pm \gamma^5)/2$ entering the $H^\pm tb$ vertex, by studying the angular behaviour of the final state particles entering single top production (recall in fact that the inclusive cross section is only proportional to the sum of the squares of such coefficients).

These aspects will constitute the subject of a separate publication.

Acknowledgments

We thank Michelangelo Mangano for his help with AlpGen and for discussions. We thank Emanuele Re for his help with POWHEG (especially for modifying the program to allow the generation without the top decaying) and for discussions. We thank Filipe Veloso for providing us with the code to extract the exclusion limits and discussions. We thank Miguel Won for help with stdhep. We thank Nuno Castro for discussions.

SM is financed in part through the NExT Institute. The work of RG and RS is supported in part by the Portuguese *Fundação para a Ciência e a Tecnologia* (FCT) under contracts PTDC/FIS/117951/2010 and PEst-OE/FIS/UI0618/2011. RG is also supported by a FCT Grant SFRH/BPD/47348/2008. RS is also partially supported by an FP7 Reintegration Grant, number PERG08-GA-2010-277025.

A. Cut flow for a 120 GeV charged Higgs boson

In table A.1 we present the cut flow for the signal ($m_{H^\pm} = 120$ GeV) and for the background starting from the trigger until cut number 5 as described in section 3. In table A.2 we show the remaining cuts numbered from 6 to 10. All numbers are efficiencies in percentage.

Process	Efficiency after cut (%)					
	Trigger	Cut 1	Cut 2	Cut 3	Cut 4	Cut 5
Signal	45.57	9.36	8.32	6.86	3.46	1.00
tj (<i>t</i>)	54.73	13.57	11.80	8.61	3.60	1.00
tj (<i>s</i>)	59.01	14.87	12.31	8.91	3.58	0.77
tj (<i>tW</i>)	80.62	25.89	21.22	11.74	5.93	1.34
<i>t</i> \bar{t} (sem)	71.15	38.34	30.47	17.11	10.63	2.57
<i>t</i> \bar{t} (lep)	84.07	43.45	26.51	14.87	11.04	2.59
<i>t</i> \bar{t} (had)	28.22	3.39	2.53	2.07	0.34	0.05
W+0j	26.14	23.50	23.50	23.36	1.05	0.01
W+1j	34.00	27.73	27.65	21.83	4.85	0.09
W+2j	38.89	28.27	28.08	19.50	5.83	0.16
W+3j	48.10	29.08	28.71	17.29	7.16	0.27
Wc+0j	41.20	35.96	35.18	25.48	4.29	0.35
Wc+1j	45.01	36.60	35.55	22.69	5.40	0.43
Wc+2j	50.37	37.46	36.07	20.34	6.72	0.54
Wc+3j	57.04	37.95	36.16	18.16	7.57	0.53
Wbb+0j	40.70	31.01	27.35	19.43	5.46	1.69
Wbb+1j	44.71	28.74	25.33	15.48	5.83	1.76
Wbb+2j	51.02	29.34	25.78	15.22	7.56	2.45
Wbb+3j	23.15	10.99	9.17	4.34	3.08	5.98×10^{-1}

Table A.1: Efficiency flow (trigger to cut 5) for a charged Higgs mass of 120 GeV.

References

- [1] G. Aad *et al.* [ATLAS Collaboration], Phys. Lett. B **710** (2012) 49.
- [2] S. Chatrchyan *et al.* [CMS Collaboration], Phys. Lett. B **710** (2012) 26.
- [3] LEP Higgs Working Group for Higgs boson searches, ALEPH, DELPHI, L3 and OPAL Collaborations, arXiv: hep-ex/0107031.
- [4] H. E. Logan and D. MacLennan, Phys. Rev. D **79** (2009) 115022.
- [5] P. Gutierrez [for the CDF and D0 Collaborations], FERMILAB-CONF-10-540-E; V. M. Abazov *et al.* [D0 Collaboration], Phys. Rev. D **80** (2009) 051107; CDF Collaboration, CDF/PUB/TOP/PUBLIC/7712.
- [6] G. Aad *et al.* [ATLAS Collaboration], arXiv:1204.2760 and ATLAS-CONF-2011-094; S. Chatrchyan *et al.* [CMS Collaboration], CMS-HIG-11-008 and CMS-HIG-11-019.
- [7] V. D. Barger, J. L. Hewett and R. J. N. Phillips, Phys. Rev. D **41** (1990) 3421.

Process	Efficiency after cut (%)				
	Cut 6	Cut 7	Cut 8	Cut 9	Cut 10
Signal	4.33×10^{-1}	1.13×10^{-1}	4.36×10^{-2}	3.94×10^{-2}	1.93×10^{-2}
tj (<i>t</i>)	2.62×10^{-1}	6.10×10^{-2}	1.62×10^{-2}	1.47×10^{-2}	7.50×10^{-3}
tj (<i>s</i>)	1.43×10^{-1}	3.67×10^{-2}	8.33×10^{-2}	6.67×10^{-3}	≈ 0
tj (<i>tW</i>)	4.58×10^{-1}	1.31×10^{-1}	1.10×10^{-3}	6.00×10^{-3}	1.00×10^{-3}
<i>t</i> \bar{t} (sem)	1.09	2.93×10^{-1}	9.12×10^{-2}	4.50×10^{-3}	≈ 0
<i>t</i> \bar{t} (lep)	7.31×10^{-1}	1.75×10^{-1}	1.95×10^{-3}	1.45×10^{-2}	2.00×10^{-3}
<i>t</i> \bar{t} (had)	4.29×10^{-2}	3.50×10^{-3}	≈ 0	≈ 0	≈ 0
W+0j	1.48×10^{-4}	≈ 0	≈ 0	≈ 0	≈ 0
W+1j	3.20×10^{-3}	7.22×10^{-4}	3.36×10^{-4}	3.07×10^{-4}	7.15×10^{-6}
W+2j	2.41×10^{-2}	5.88×10^{-3}	2.33×10^{-3}	2.19×10^{-3}	1.39×10^{-4}
W+3j	9.51×10^{-2}	2.15×10^{-2}	7.58×10^{-4}	5.89×10^{-4}	≈ 0
Wc+0j	3.93×10^{-3}	5.74×10^{-4}	8.19×10^{-5}	8.19×10^{-5}	≈ 0
Wc+1j	4.63×10^{-2}	7.33×10^{-3}	3.54×10^{-3}	3.54×10^{-3}	1.01×10^{-3}
Wc+2j	1.18×10^{-1}	2.45×10^{-2}	5.32×10^{-3}	2.13×10^{-3}	1.06×10^{-3}
Wc+3j	1.92×10^{-1}	5.49×10^{-2}	2.74×10^{-3}	≈ 0	≈ 0
Wbb+0j	1.31×10^{-1}	2.95×10^{-2}	2.11×10^{-2}	2.11×10^{-2}	≈ 0
Wbb+1j	3.35×10^{-1}	1.05×10^{-1}	4.19×10^{-2}	3.49×10^{-2}	6.98×10^{-3}
Wbb+2j	7.80×10^{-1}	1.89×10^{-1}	≈ 0	≈ 0	≈ 0
Wbb+3j	2.99×10^{-1}	6.90×10^{-2}	≈ 0	≈ 0	≈ 0

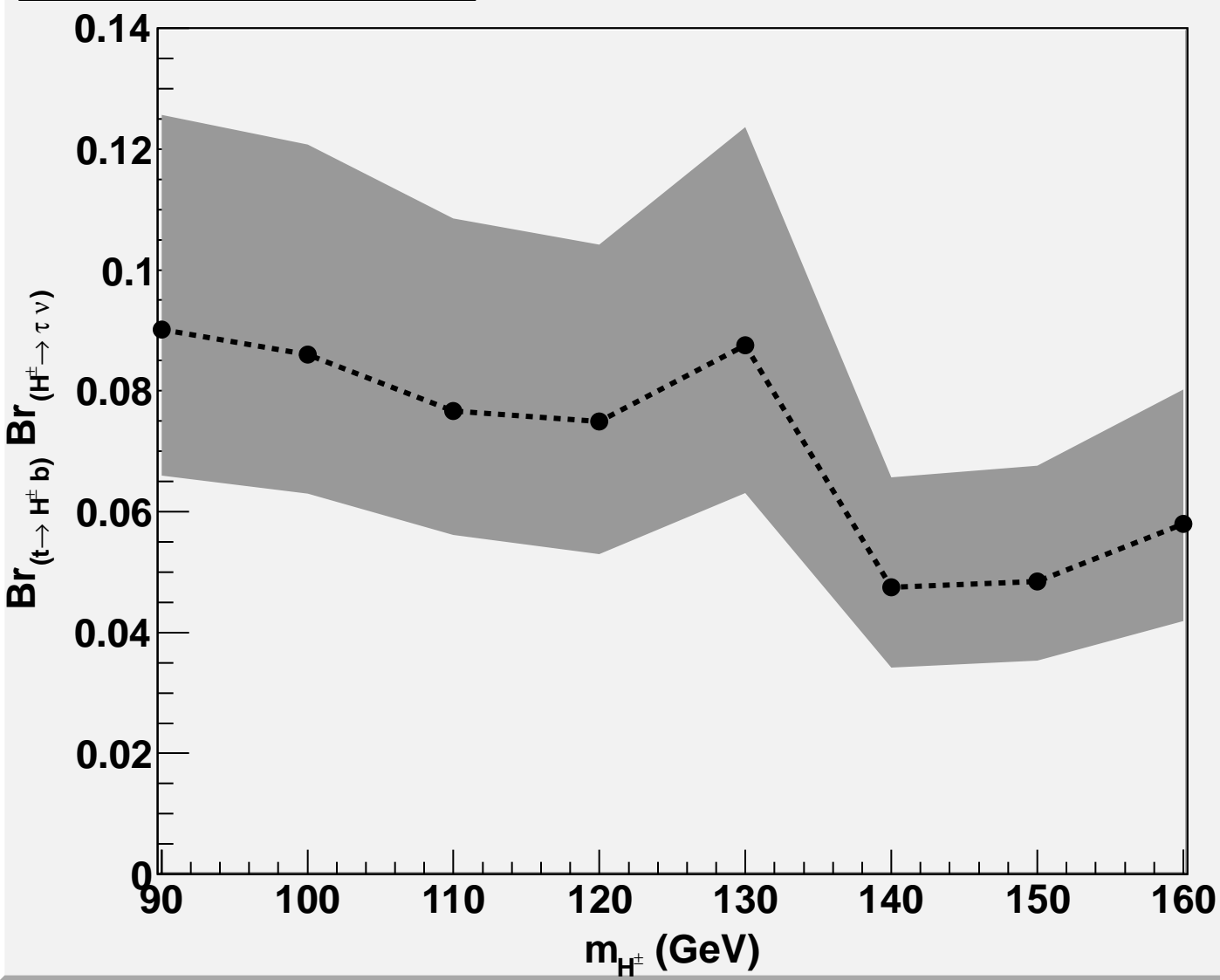
Table A.2: Efficiency flow (cut 6 to cut 10) for a charged Higgs mass of 120 GeV.

- [8] M. Aoki, S. Kanemura, K. Tsumura and K. Yagyu, Phys. Rev. D **80** (2009) 015017.
- [9] W. S. Hou and R. S. Willey, Phys. Lett. B **202** (1988) 591; M. Ciuchini, G. Degrandi, P. Gambino and G. F. Giudice, Nucl. Phys. B **527** (1998) 21; F. Borzumati and C. Greub, Phys. Rev. D **58** (1998) 074004 and ibidem **59** (1999) 057501; C. Amsler *et al.*, Phys. Lett. B **667** (2008) 1; The Belle Collaboration, Phys. Rev. Lett. **103** (2009) 241801.
- [10] S. Su and B. Thomas, Phys. Rev. D **79** (2009) 095014.
- [11] M. Aoki, R. Guedes, S. Kanemura, S. Moretti, R. Santos and K. Yagyu, Phys. Rev. D **84** (2011) 055028; R. Guedes, S. Kanemura, S. Moretti, R. Santos and K. Yagyu, PoS CHARGED **2010** (2010) 037.
- [12] M. Aoki, S. Kanemura and O. Seto, Phys. Rev. Lett. **102** (2009) 051805 and Phys. Rev. D **80** (2009) 033007; M. Aoki, S. Kanemura and K. Yagyu, arXiv:1102.3412 [hep-ph]; H. S. Goh, L. J. Hall and P. Kumar, JHEP **0905** (2009) 097.
- [13] N. Kidonakis, Phys. Rev. D **82** (2010) 054018.

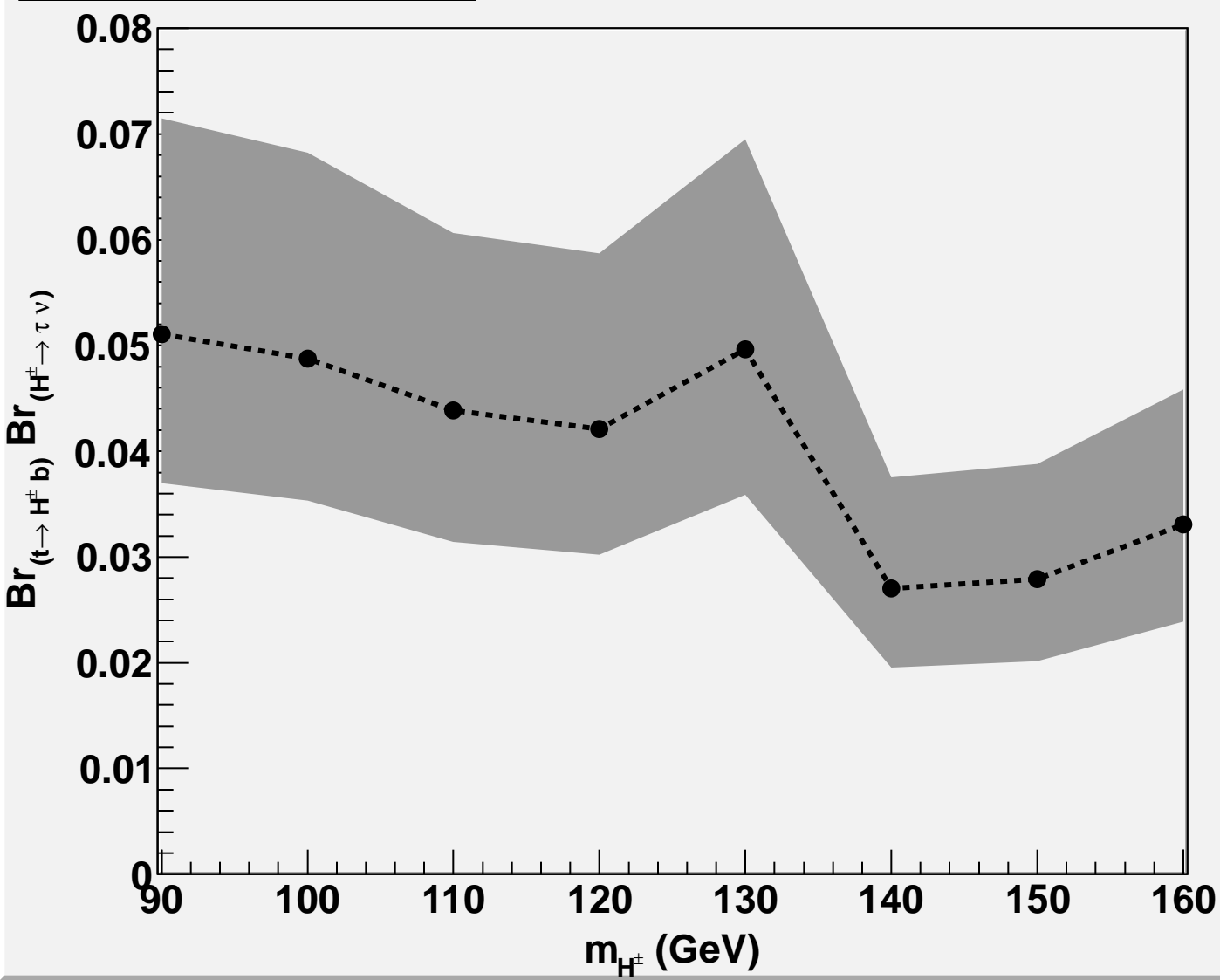
- [14] N. Kidonakis, Phys. Rev. D **81** (2010) 054028.
- [15] N. Kidonakis, Phys. Rev. D **83** (2011) 091503.
- [16] A. D. Martin, W. J. Stirling, R. S. Thorne and G. Watt, Eur. Phys. J. C **63** (2009) 189.
- [17] S. Alioli, P. Nason, C. Oleari and E. Re, JHEP **1006** (2010) 043; S. Alioli, P. Nason, C. Oleari and E. Re, JHEP **0909** (2009) 111 [Erratum-ibid. **1002** (2010) 011]; E. Re, Eur. Phys. J. C **71** (2011) 1547; S. Frixione, P. Nason and G. Ridolfi, JHEP **0709** (2007) 126; P. Nason, JHEP **0411** (2004) 040; S. Frixione, P. Nason and C. Oleari, JHEP **0711** (2007) 070.
- [18] P. M. Nadolsky *et al.*, Phys. Rev. D **78** (2008) 013004.
- [19] T. Sjostrand, S. Mrenna and P. Z. Skands, JHEP **0605** (2006) 026.
- [20] M. L. Mangano, M. Moretti, F. Piccinini, R. Pittau and A. D. Polosa, JHEP **0307** (2003) 001.
- [21] A. Pukhov, arXiv:hep-ph/0412191.
- [22] P. Z. Skands, arXiv:0905.3418 [hep-ph].
- [23] The ATLAS Collaboration, ATL-PHYS-PUB-2010-002.
- [24] B. P. Kersevan and E. Richter-Was, arXiv:hep-ph/0405247.
- [25] J. M. Campbell and R. K. Ellis, Phys. Rev. D **60** (1999) 113006.
- [26] Code available from <http://mcfm.fnal.gov/>.
- [27] M. Mangano, *Merging multijet matrix elements and shower evolution in hadronic collisions*, <http://cern.ch/%7Emlm/talks/lund-alp-gen.pdf> (2004).
- [28] S. Ovin, X. Rouby and V. Lemaitre, arXiv:0903.2225 [hep-ph].
- [29] V. Barger and R. J. N. Phillips, *Collider Physics*, Addison-Wesley Publishing Company, 1997.
- [30] J. M. Campbell, R. K. Ellis and D. L. Rainwater, Phys. Rev. D **68** (2003) 094021.
- [31] F. M. A. Veloso, CERN-THESIS-2008-106.
- [32] G. Aad *et al.* [ATLAS Collaboration], JHEP **1206** (2012) 039 [arXiv:1204.2760 [hep-ex]]; ATLAS collaboration, talk given by Aldo F. Saavedra at ICHEP2012 (2012).
- [33] S. Chatrchyan *et al.* [CMS Collaboration], JHEP **1207** (2012) 143 [arXiv:1205.5736 [hep-ex]]; CMS collaboration, talk given by Christian Veelken at ICHEP2012 (2012).
- [34] G. C. Branco, P. M. Ferreira, L. Lavoura, M. N. Rebelo, M. Sher and J. P. Silva, Phys. Rept. **516** (2012) 1 [arXiv:1106.0034 [hep-ph]].

- [35] P. M. Ferreira, R. Santos and A. Barroso, Phys. Lett. B **603** (2004) 219 [Erratum-ibid. B **629** (2005) 114].
- [36] I. F. Ginzburg, M. Krawczyk and P. Osland, hep-ph/0211371.
- [37] A. W. El Kaffas, W. Khater, O. M. Ogreid and P. Osland, Nucl. Phys. B **775** (2007) 45 [hep-ph/0605142].
- [38] A. Arhrib, E. Christova, H. Eberl and E. Ginina, JHEP **1104** (2011) 089.
- [39] A. Barroso, P. M. Ferreira, R. Santos and J. P. Silva, arXiv:1205.4247 [hep-ph].
- [40] L. Basso, A. Lipniacka, F. Mahmoudi, S. Moretti, P. Osland, G. M. Pruna and M. Pirmohammadi, arXiv:1205.6569 [hep-ph].
- [41] G. Aad *et al.* [ATLAS Collaboration], arXiv:0901.0512 [hep-ex].
- [42] CMS Collaboration, Physics Technical Design Report, Volume 2. CERN/LHCC 2006-021.

Luminosity: 10 fb⁻¹



Luminosity: 30 fb⁻¹



Luminosity: 300 fb^{-1}

